



1 **Volcanic imprint in the North Atlantic climate**
2 **variability as recorded by stable water isotopes of**
3 **Greenland ice cores**
4

5 Hera Guðlaugsdóttir¹, Jesper Sjolte², Árný Erla Sveinbjörnsdóttir¹ and Hans Christian
6 Steen-Larsen³

7
8 ¹Nordic Volcanological Centre (NordVulk), Institute of Earth Sciences, University of Iceland

9 ²Department of Geology, Lund University

10 ³Geophysical Institute, University of Bergen and Bjerknes Centre for Climate Research, Bergen,
11 Norway

12
13 *Correspondence to: Hera Guðlaugsdóttir (hera@hi.is)*
14

15 **Abstract.** Volcanic eruptions are important drivers of climate variability on both seasonal and multi-
16 decadal time scales as a result of atmosphere-ocean coupling. While the direct response after equatorial
17 eruptions emerges as the positive phase of the North Atlantic Oscillation in the first two years after an
18 eruption, less is known about high latitude northern hemisphere eruptions. In this study we assess the
19 difference between equatorial and high latitude volcanic eruptions through the reconstructed
20 atmospheric circulation and stable water isotope records of Greenland ice cores for the last millennia
21 (1241-1979 CE), where the coupling mechanism behind the long-term response is addressed. The
22 atmospheric circulation is studied through the four main modes of climate variability in the North
23 Atlantic, the Atlanti Ridge (AtR), Scandinavian Blocking (ScB) and the positive and negative phase of
24 the North Atlantic Oscillation (NAO+/NAO-). We report a difference in the atmospheric circulation
25 response after equatorial eruptions compared to the response after high latitude eruptions, where NAO+
26 and AtR seem to be more associated with equatorial eruptions while NAO- and ScB seems to follow
27 high latitude eruptions. This response is present during the first five years and then again in years 8-12
28 after both equatorial and high latitude eruptions. Such a prolonged response is evidence of an ocean-
29 atmosphere coupling that is initiated through different mechanisms, where we suspect sea ice to play a
30 key role.

31
32 **1 Introduction**
33

34 Climate variability is mainly subjected to variations in energy and mass transfers within the Earth's
35 atmosphere that further drive the internal dynamic forcing within the climate system. The main factors
36 that can have a profound impact on this energy/mass transfer are anthropogenic and volcanic forcing,
37 where the latter one is the scope of this study. Due to the physical properties of volcanic sulfate
38 aerosols, formed when SO₂ from the eruptive plume reacts with water in the atmosphere, incoming
39 short-wave solar radiation is scattered while long-wave terrestrial radiation is absorbed. For eruptions
40 with an eruptive column reaching up into the stratosphere, this can be manifested as variations in the
41 temperature gradients of the Earth's atmosphere, both in the vertical and latitudinal direction, that
42 further continue to influence the atmospheric circulation and pressure systems. It is well known that



43 large equatorial eruptions increase the temperature gradient in the stratosphere that can lead to
44 amplification of the formation and transport of planetary waves (Graf et al., 1994, Kodera, 1994). In
45 turn, the stratospheric zonal winds are known to increase and manifest in the tropospheric climate
46 variability of the Northern Hemisphere as the positive phase of the North Atlantic Oscillation (NAO+),
47 one of the main modes of climate variability in the North Atlantic, in the first two winters after an
48 eruption (Robock and Mao, 1992; Graf et al., 1994, Kodera, 1994; Fisher et al., 2007; Ortega et al.,
49 2015). Other two modes of the North Atlantic (NA) climate variability, described through the third and
50 fourth EOFs of SLP (Wallace and Gutzler, 1981; Hurrell et al., 1995; Cassou et al., 2004), are the
51 Atlantic Ridge (AtR) and the Scandinavian Blocking (ScB) respectively. As well as having been
52 identified in the EOFs of SLP, these four modes have also been identified as being an important part of
53 the variability recorded in the isotope records of Greenland ice cores (Ortega et al., 2014). Stable water
54 isotopes (^{18}O and ^2H) in the hydrological cycle preserve information regarding their transport in the
55 atmospheric circulation as well as other climatic parameters like temperature (Johnsen et al., 2001).
56 This information can both be retrieved from daily to monthly samples of precipitation as well as on a
57 centennial to millennial time scales from e.g. Greenland ice cores (Jouzel et al., 1997; Petit et al.,
58 1999). Usually when referring to stable water isotopes, the delta (δ) notation is used where the sample
59 value is compared to a known standard, usually Standard Mean Ocean Water (SMOW), that results in
60 values expressed in parts per thousand (‰).

61 High latitude (North Hemisphere, NH) volcanic eruptions have been less studied when it comes to the
62 impact on the main NA climate modes. However in a model study by Guðlaugsdóttir et al. (2018) it
63 was shown that NH eruptions have a slight tendency to force the atmospheric circulation towards the
64 negative phase of NAO (NAO-) as a result of a weakening of the stratospheric zonal winds. This
65 response was detected in the first 2-4 years as well as around a decade after an eruption where the study
66 of Guðlaugsdóttir et al. (2019) provided further evidence to support this. It has been shown that, as well
67 as EQ volcanic eruptions (Ottera et al., 2010; Swingedouw et al., 2015), NH volcanic eruptions too
68 have the ability to impact climate through the Atlantic Meridional Overturning Circulation (AMOC)
69 and ENSO on decadal to multi-decadal timescales (Pausata et al., 2015). However, much is still to be
70 learnt about the controlling mechanism behind the climate impact after NH volcanic eruptions. In this
71 study we compare the atmospheric winter circulation response after both EQ and NH volcanic
72 eruptions by analyzing 20 post-volcanic winters (referred to here as years). We assess the winter
73 circulation through the four main modes of NA climate variability in order to get more quantitative
74 information regarding the atmospheric circulation.

75 In this study we take advantage of the information that can be obtained from the stable water isotope
76 records of multiple Greenland ice cores. We hypothesize that the climate response after volcanic
77 eruptions can be detected in the $\delta^{18}\text{O}$ records of Greenland ice cores. This involves both the direct
78 climate response due to changes in solar insolation as well as the indirect dynamical climate response
79 that indicate interactions between the main components of the climate system, the atmospheric
80 circulation, ocean and sea ice. We first study the volcanic response 1-5 years after each eruption in 13
81 shallow Greenland ice cores spanning the period 1771-1970 CE with the aim to retrieve spatial $\delta^{18}\text{O}$
82 pattern over the ice sheet that is associated with the atmospheric circulation response after both



83 equatorial and high latitude (North Hemisphere) volcanic eruptions. To compliment the information
84 identified in these records, the reconstructed SLP and surface temperature at 2 meters (T2m) for the
85 same period are also analyzed. The pattern that emerges is then tested further using longer time series,
86 now using three Greenland ice cores as well as the reconstruction fields, for the period of 1241-1970
87 CE to study 1-20 years after volcanic eruptions. A final assessment on the volcanic response identified
88 is then done by analyzing the average accumulation rates of three shallow North Greenland ice cores.

89

90 **2 Data & Methods**

91

92 **2.1 Greenland ice cores**

93 To investigate the volcanic response in $\delta^{18}\text{O}$ of Greenland ice cores, we use the winter seasonal means
94 (Nov-April) of 13 Greenland ice cores spanning the period 1771-1970 CE (Vinther et al., 2010). To
95 assess a long-term volcanic response 1-20 years after an eruption the winter seasonal mean response is
96 investigated in 3 Greenland ice cores, Dye 3, GRIP and Crete, spanning the period of 1241-1978 CE
97 (Vinther et al., 2010). Due to issues with the ice core chronology prior to ~1000 CE (Sigl et al., 2015),
98 and to keep consistency between the ice core and reconstruction analysis, we do not analyze volcanic
99 eruptions prior to 1241 CE.

100

101 **2.2 Reconstruction of the NA atmospheric winter circulation**

102 To further assess the spatial and temporal volcanic signal in the $\delta^{18}\text{O}$ of Greenland ice cores, both the
103 short and long-term volcanic signal is investigated in the NA atmospheric winter circulation
104 reconstructions of Sjolte et al. (2018). The reconstruction is conducted by using an isotope-enabled
105 version of the atmosphere-ocean model ECHAM5/MPI-OM (Werner et al., 2016) where the period
106 800-2000 CE is simulated. By using 8 seasonally resolved Greenland ice cores for the period 1241-
107 1970 CE and simulated $\delta^{18}\text{O}$, each year in the ice core data is matched with the model data by methods
108 described in Sjolte et al. (2018). This results in 39 significant model fits that are used to reconstruct the
109 atmospheric pressure, temperature at 2m (T2m) and $\delta^{18}\text{O}$ fields for the period 1241-1970. The forcing
110 that is implemented in the model is the same as in Jungclaus et al. (2010), except that the solar forcing
111 has been updated (Muscheler et al., 2016). Since our purpose is to be able to identify specific weather
112 regimes as a result of volcanic eruptions, it is important to have a reference. The reconstructed surface
113 pressure was clustered in the attempt to retrieve the four main weather regimes in the NA but without
114 success. Therefore the surface pressure (referred to as SLP) in ECHAM5-wiso was clustered using a k-
115 means clustering method where the centers were pre-defined to be 4 ($k=4$) according to Cassou et al.
116 (2004). To retrieve the most stable centroids, the calculation of cluster centroids was repeated 100
117 times. We also use the $\delta^{18}\text{O}$ pattern associated with the weather regimes identified in the 500mb gph of
118 ECHAM5-wiso that has previously been retrieved by authors (Guðlaugsdóttir et al., 2019). Although
119 we are not studying the 500mb gph, this provides the best estimate we have regarding the $\delta^{18}\text{O}$ pattern
120 that is associated with the weather regimes identifiable in the reconstructed $\delta^{18}\text{O}$ anomaly fields
121 ($\delta^{18}\text{O}_{\text{reconst}}$). In order for a post volcanic year to be assigned with a specific weather regime, we use r



122 ≥ 0.4 and $p < 0.01$ as a reference where the correlation tables are given in the supplementary. This
 123 applies both for $\delta^{18}\text{O}$ and surface pressure fields.

124

125 2.3 Extracting volcanic signal

126 We select 5 equatorial (EQ) eruptions and 5 North Hemisphere (NH) eruptions to assess the volcanic
 127 response 0-5 years after an eruption in $\delta^{18}\text{O}$ anomalies of 13 Greenland ice cores ($\delta^{18}\text{O}_{\text{ice}}$) as well as in
 128 the reconstructed atmospheric pressure, T2m and $\delta^{18}\text{O}_{\text{reconst}}$.

129 The response using 3 Greenland ice cores is also assessed along with the associated reconstruction
 130 fields with the aim to retrieve the long-term (1-20 years after an eruption). The years that are presented
 131 in the results are selected from the average $\delta^{18}\text{O}_{\text{ice}}$ calculated from all three cores and where the
 132 significance is by implementing a statistical Monte Carlo approach. The number of volcanic eruptions
 133 used is presented in Table 1. The significance of the signal extracted from each core as well as
 134 reconstructions is assessed at the 90 and 95% confidence level using a two-tailed Student's t-test, where
 135 n is the number of volcanic eruptions stacked.

136

137 Table 1: List of all volcanic eruptions analyzed in each part. *Sigl et al. (2015)

Eruption	Eruption year	1241-1978 CE (<i>year</i> 1 – 5) ($n=8$)	1241-1978 CE (<i>year</i> 8 – 20) ($n=8$)	1771-1970 CE (<i>year</i> 0 – 5) ($n=5$)	1724-2011 CE (<i>NEEM</i>) ($n=6$)	Forcing* (W/m^2)
Equatorial						
Samalas	1258	x	x			-32.8
Unknown	1276	x	x			-7.7
Unknown	1345	x	x			-9.4
Kuawe	1458	x	x			-20.1
Huyaputina	1601	x	x			-11.6
Parker	1641	x	x			-11.8
Banda Api	1695	x	x			-10.2
Unknown	1809			x	x	-12.0
Tambora	1815	x	x	x		-17.2
Cosiguina	1836			x	x	-6.6
Krakataua	1884			x	x	-5.5
Agung	1963			x	x	-3.8 (1964)
El Chichon	1982				x	-0.4
Pinatubo	1991				x	-6.5 (1992)
NH						
Hekla	1300	x	x			–
Öraefajökull	1362	x	x			–
Veidivötn	1477	x	x			-3.1
Katla	1721	x	x			-0.8
Katla	1755	x	x		x	-0.9 (1756)
Hekla	1766				x	-1.4
Laki	1783	x	x	x	x	-15.5
Askja	1875	x		x	x	-0.6
Novarupta	1912			x		-3.3
Katla	1918			x		-0.7 (1919)
Hekla	1947	x	x	x	x	-0.6
Hekla	1970				x	–

138

139 The EQ eruptions are selected based on Sigl et al. (2015) where the individual eruptions selected do not
 140 interfere with one another within the time frame analyzed (either 1-5 or 1-20 years). The radiative
 141 forcing for the EQ eruptions is between -3.8W/m^2 and -32.8W/m^2 with the exception of El Chichon
 142 that is -0.4W/m^2 . However since it is considered to be one of the largest eruptions of the 20th century it
 143 is included. It can be difficult to select an ideal candidate for the analysis of the climate response after
 144 NH eruptions since they do occur frequently but few have the ability to alter the climate system. Many



145 of the NH volcanic eruptions that have been selected in Table 1 are considered to be one of the largest
146 volcanic eruptions in the last millennium, where all but one NH eruption listed in the table is Icelandic.
147 Some of these eruptions erupted for a year or more (Hekla 1300 and 1766) others lasted a little less
148 than a year (Laki 1783 and Askja 1875) although the duration of the majority of the eruptions is 1-5
149 months (Janebo et al., 2016; Carey et al., 2009; Thordarson et al., 2003; Thordarson and Larsen, 2007;
150 Sharma et al., 2008). We also use the reconstructed forcing by Sigl et al. (2015) to select these NH
151 eruptions except for two events, the Hekla 1300 and Örfajökull 1362. Hekla 1300 CE lasted a year
152 and has been assigned a VEI index of 4 while Örfajökull erupted for several months (June-Oct) with a
153 VEI index of 5-6.

154

155 **3 Results**

156

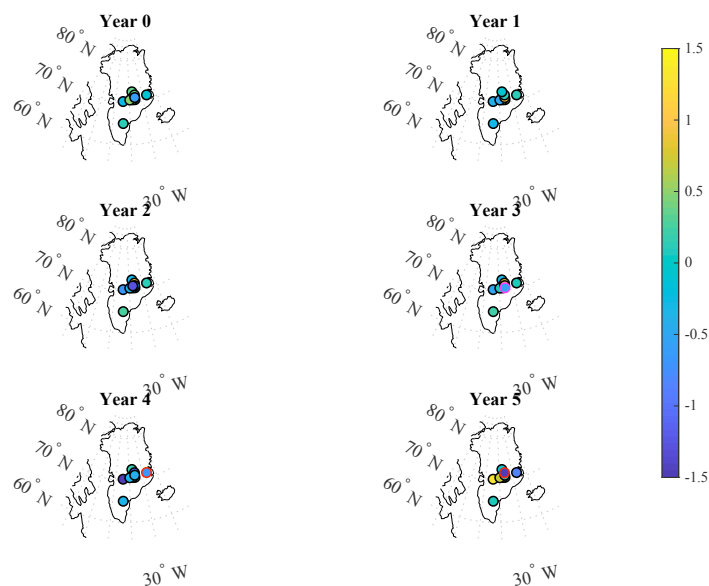
157 **3.1 Equatorial volcanic response**

158

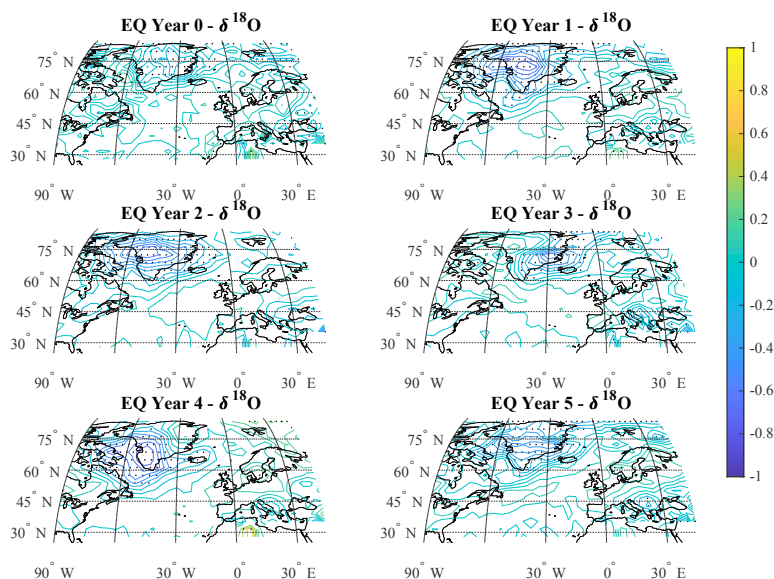
159 **3.1.1 Atmospheric circulation response 0-5 years after EQ eruptions: 1771-1970 CE**

160 Figures 1-3 show results for the atmospheric circulation response 0-5 years (winters) after EQ volcanic
161 eruptions. Since year 0 is the year of the volcanic eruptions, it includes little volcanic perturbations but
162 is kept for comparison. It is however displayed for comparison. The volcanic eruptions were selected
163 according to Table 1, where 5 volcanic eruptions were stacked in $\delta^{18}\text{O}_{\text{ice}}$ of 13 cores, as well as
164 $\delta^{18}\text{O}_{\text{reconst}}$ and surface pressure reconstructions, to retrieve a composite anomaly signal calculated with
165 respect to 10 years prior to each event. See T2m post volcanic fields in supplementary Figure F2. To
166 assess the post-volcanic reconstruction fields, we use the average $\delta^{18}\text{O}$ and surface pressure pattern
167 (supplementary Figure F1) associated with each weather regime that has been retrieved from
168 ECHAM5-wiso (supplementary Table T1-T2).

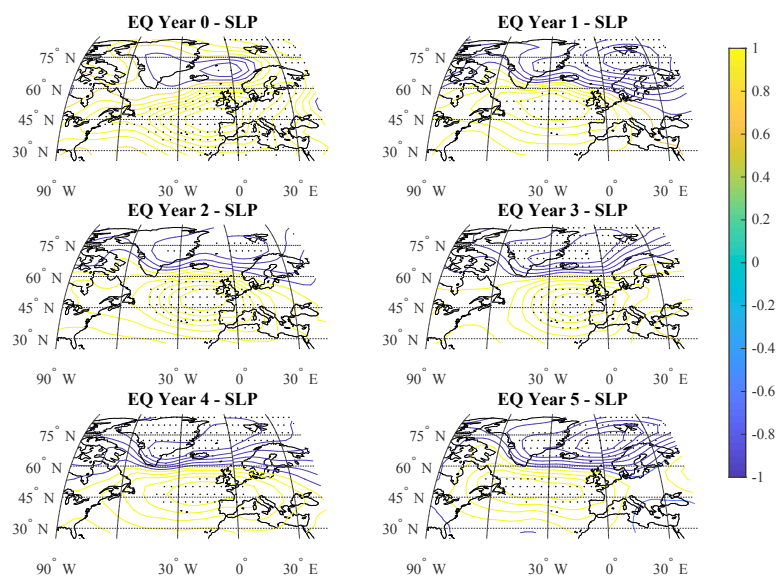
169



170
171 Figure 1: Composite $\delta^{18}\text{O}_{\text{ice}}$ anomalies of 13 Greenland ice cores (1771-1970 CE) 0-5 years after 5
172 equatorial volcanic eruptions. Magenta circles (years 1 and 2) are sites with significance at the 90%
173 confidence level and red circles (years 4 and 5) are sites with significance at the 95% confidence level.
174



175
176 Figure 2: The short-term $\delta^{18}\text{O}_{\text{reconst}}$ response 0-5 years after 5 EQ volcanic eruptions.
177



178
179 Figure 3: The short-term surface pressure response 0-5 years after 5 EQ volcanic eruptions.

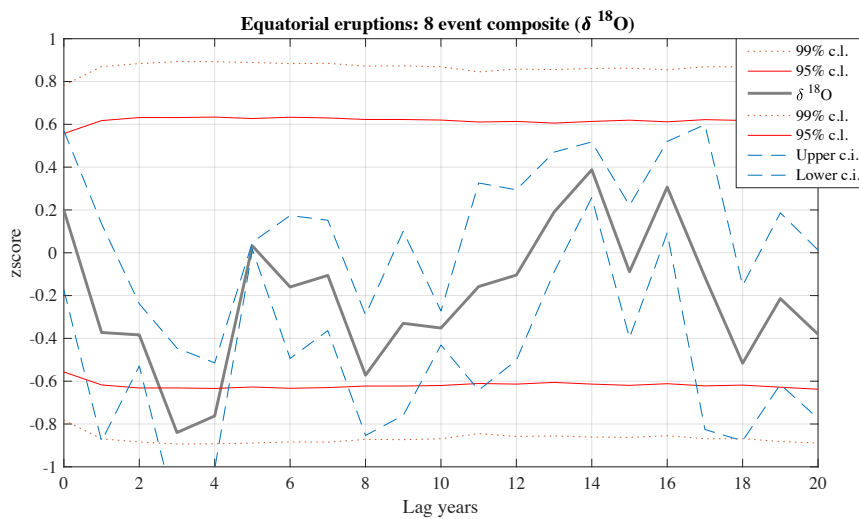
180
181 A general agreement can be found between the spatial $\delta^{18}\text{O}_{\text{ice}}$ pattern identified in Figure 1 and the
182 $\delta^{18}\text{O}_{\text{reconst}}$ pattern over Greenland in Figure 2 for all years with year 5 being an exception. A clear
183 atmospheric circulation response emerges in years 1-5 in all parameters analyzed, where $\delta^{18}\text{O}_{\text{ice}}$
184 becomes significant in year 3 at the 90% c.i. and year 4-5 at the 95% c.i. The $\delta^{18}\text{O}_{\text{ice}}$ anomaly pattern in
185 years 3-4 is on average negative while a gradient is present in year 5 with more positive anomalies in
186 SW-Greenland that become more negative towards NE. When compared with the $\delta^{18}\text{O}$ pattern
187 associated with each weather regime, this indicates the presence of NAO+. While $\delta^{18}\text{O}_{\text{reconst}}$ is less clear
188 on this, with a weak correlation with AtR in year 3 ($r=0.37$) while years 1-2 and 4-5 correlates with
189 NAO+ ($r=0.49-0.67$, $p<0.01$), the SLP shows a clear NAO+ pattern present in all years 1-5 ($r>0.7$ and
190 $p<0.01$). This is also detected in the T2m (supplementary Figure F2).

191
192 **3.1.2 Atmospheric circulation response 1-4, 8-11 and 17-20 years after EQ eruptions: 1241-1978**
193 **CE.**

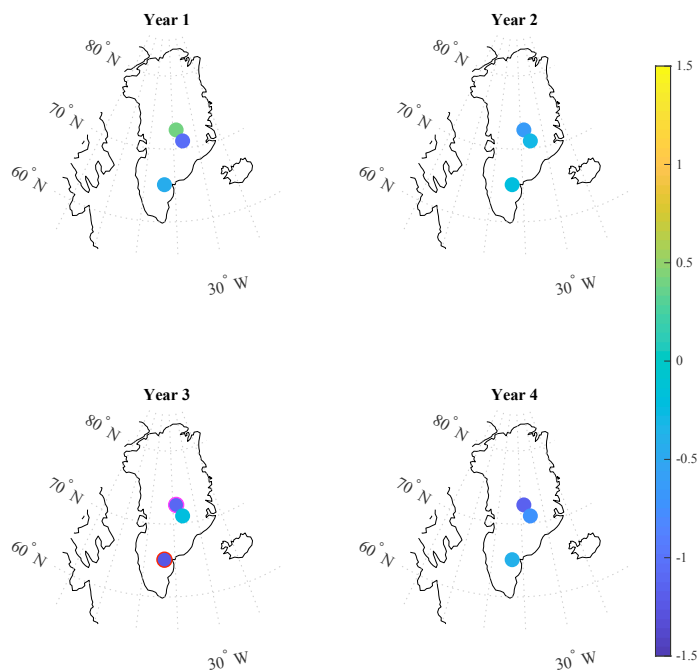
194 Figures 4-6 show results for the atmospheric circulation response where the significant years detected
195 in the 3-core average (Figure 4a) have been retrieved from the reconstruction fields and their anomalies
196 calculated with respect to 10 years prior each event. The volcanic eruptions were selected according to
197 Table 1, where 8 volcanic eruptions were stacked in $\delta^{18}\text{O}$ of 3 cores ($\delta^{18}\text{O}_{\text{ice}}$), as well as in the $\delta^{18}\text{O}_{\text{reconst}}$
198 and SLP fields to retrieve a composite anomaly signal 1-4, 8-11 and 17-20 years after EQ eruptions.
199 See T2m post volcanic fields in supplementary Figure F3. To assess the post-volcanic reconstruction
200 fields, we use the average $\delta^{18}\text{O}$ and surface pressure pattern that is associated with each weather regime
201 (supplementary Table T1-T2).
202



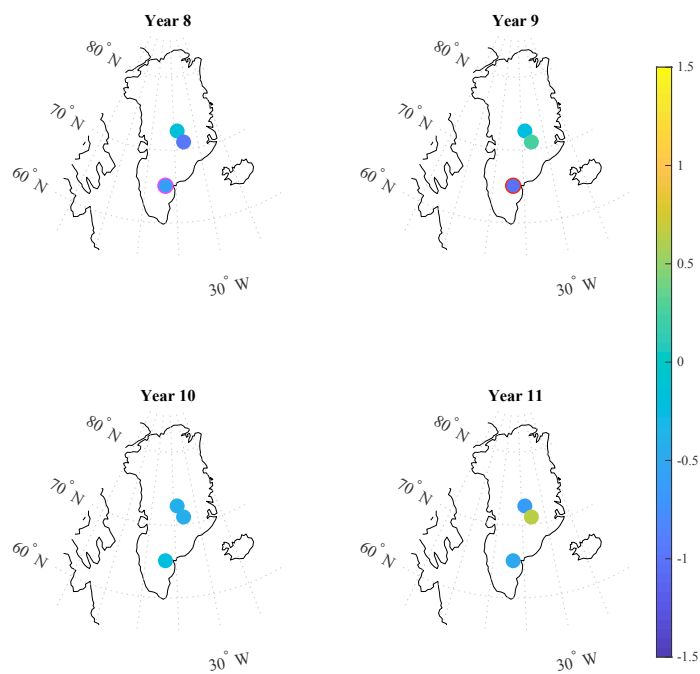
203 a)
204



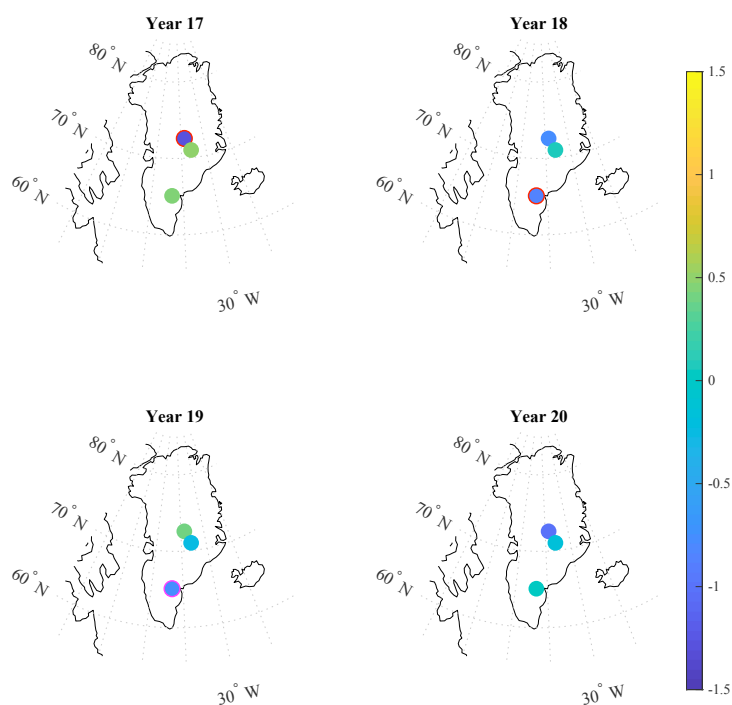
205
206
207
208 b)



209
210 c)



211
212 d)
213

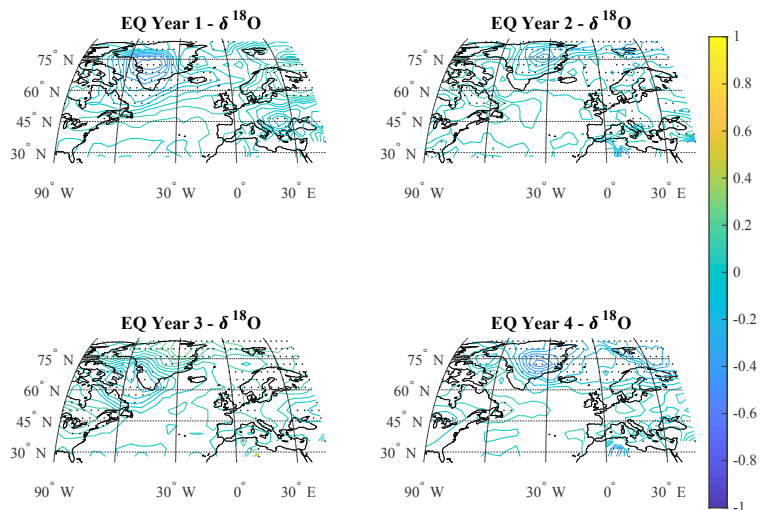


214
215
216
217
218
219
220
221
222
223
224
225
226
227
228
229
230
231
232
233
234

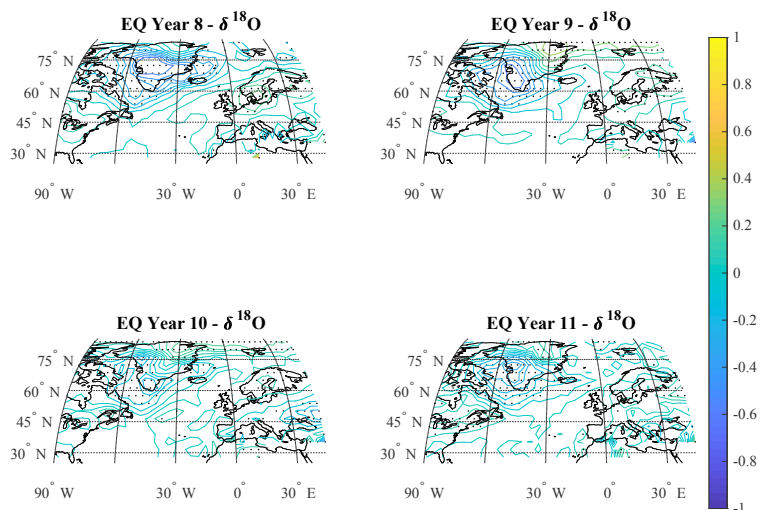
Figure 4: a) The average $\delta^{18}\text{O}$ of all three ice cores (Dye 3, GRIP and Crete). Based on significant years in a) the $\delta^{18}\text{O}$ response in years 1-4 (b), years 8-11 (c) and years 17-20 (d) is shown where number of EQ volcanic eruptions in the period of 1241-1978 CE is 8.



235 a)



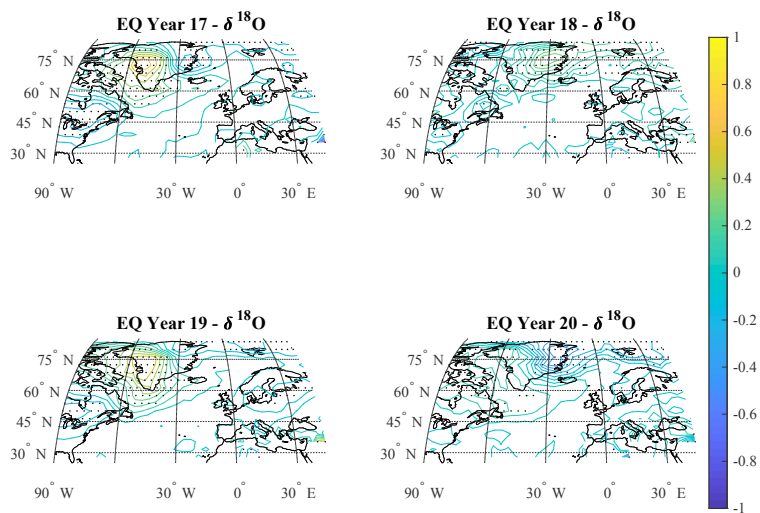
236
237 b)



238
239
240
241
242
243
244
245
246
247



248 c)

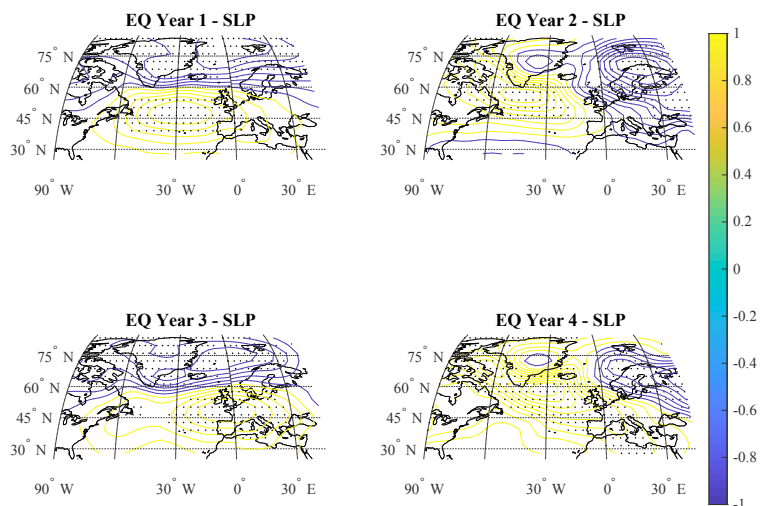


249

250 Figure 5: The composite $\delta^{18}\text{O}_{\text{reconst}}$ response a) 1-4 years, b) 8-11 years and c) 17-20 years after 8 EQ
251 volcanic eruptions.

252

253 a)



254

255

256

257

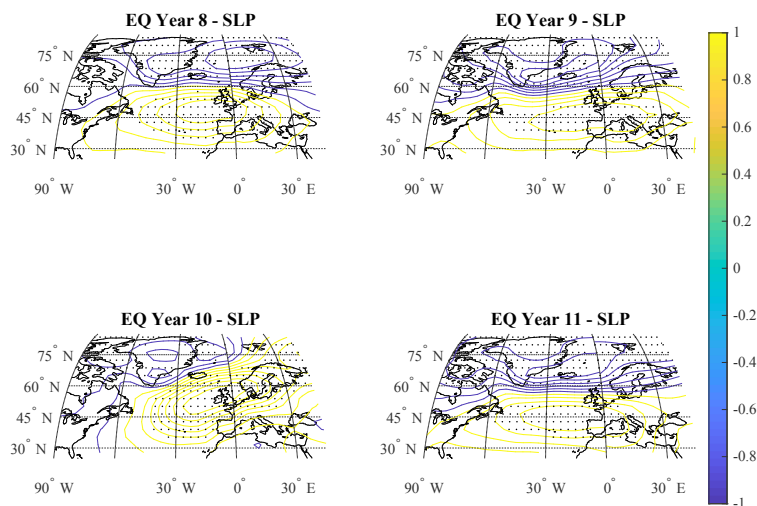
258

259

260

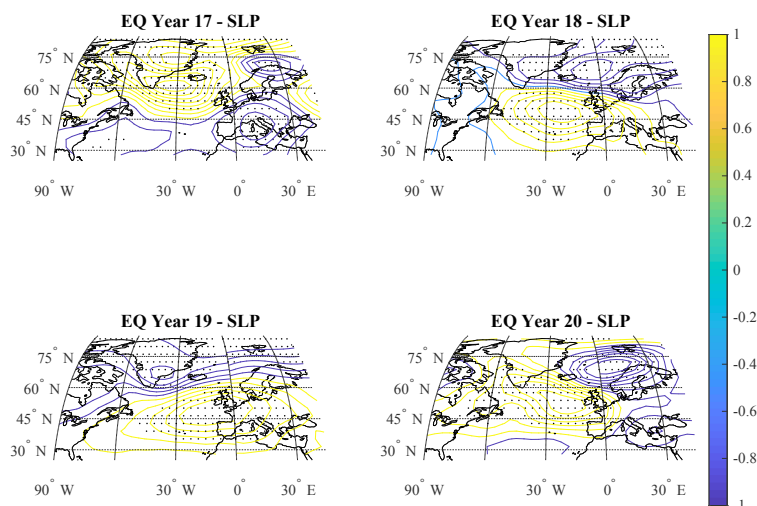


261 b)



262

263 c)



264

265

266 Figure 6: The composite SLP response a) 1-4 years, b) 8-11 years and c) 17-20 years after 8 EQ
267 volcanic eruptions.

268

269 The $\delta^{18}\text{O}_{\text{ice}}$ pattern in Figure 4 is consistent with the $\delta^{18}\text{O}_{\text{reconst}}$ pattern for all years except year 3 where
270 positive anomalies are present while $\delta^{18}\text{O}_{\text{ice}}$ show negative anomalies that are significant in the 95%
271 (Dye 3) and 90% (GRIP) c.l. A persistent NAO+ pattern is present in both $\delta^{18}\text{O}_{\text{ice}}$ and SLP in years 8-
272 11 in Figure 5b and 6b except for ScB being present in reconstructed $\delta^{18}\text{O}$ in year 10 ($r=0.57$).
273 Negative anomalies are present in $\delta^{18}\text{O}_{\text{ice}}$, of which year 8 is significant in the 90% c.l. and year 9 in the



274 95% c.l. that strongly supports such a prolonged NAO+ signal. This is further supported in the T2m
275 fields (Figure F3).

276 Figure 5 shows a clear NAO+ response in $\delta^{18}\text{O}_{\text{reconst}}$ in years 1 ($r=0.54$) and 3 ($r=0.53$) and an AtR in
277 year 2 ($r=0.60$) and 4 ($r=0.64$) that is supported by the SLP in Figure 6 as well as in the T2m fields of
278 Figure F3. During an NAO+, negative anomalies are to be expected over Greenland. Since this pattern
279 is present in all years of Figure 5a and 6a, it is difficult to distinguish between NAO+ and AtR in the
280 ice cores (Figure 4a) since more spatial data would be required to identify AtR.

281 Years 17-20 (Figure 5c and 6c) do not show as much consistency between $\delta^{18}\text{O}_{\text{reconst}}$ and SLP
282 compared to prior years analyzed. However, year 17 shows a clear NAO- in both $\delta^{18}\text{O}_{\text{reconst}}$ ($r=0.71$)
283 and SLP ($r=0.75$). $\delta^{18}\text{O}_{\text{ice}}$ of year 17 is in support of an NAO- being present where $\delta^{18}\text{O}$ of GRIP result
284 in a 95% significant negative anomaly while the other two are slightly more positive (although
285 insignificant). The same site is also significant at the 95% c.l. (with negative anomaly) in year 18 but
286 this is not in agreement with the ScB pattern that is present in $\delta^{18}\text{O}_{\text{reconst}}$ ($r=0.55$), showing positive
287 anomalies being present over Greenland ice sheet, also confirmed in the T2m fields (Figure F3).

288

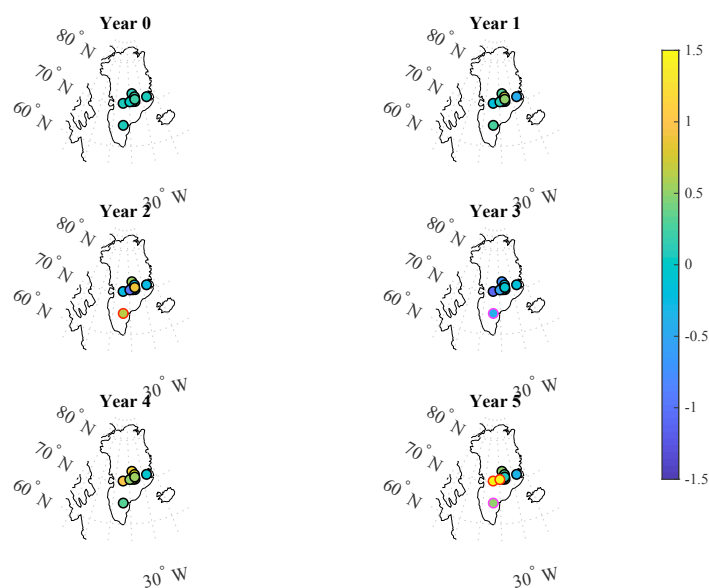
289 3.2 North Hemisphere volcanic response

290

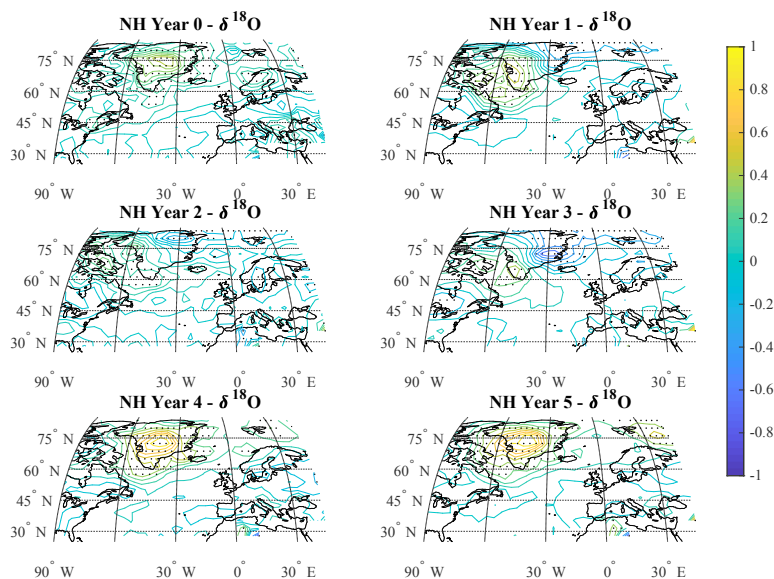
291 3.2.1 Atmospheric circulation response 0-5 years after NH eruptions: 1771-1970 CE

292 Figures 7-9 show the atmospheric circulation response after 5 composite North Hemisphere (NH)
293 volcanic eruptions where the anomalies are calculated with respect to 10 years prior to each event. As
294 for the EQ eruptions, year 0 is the eruption year and thus has little volcanic perturbations but is kept
295 here for comparison. The volcanic eruptions were selected according to Table 1, where the volcanic
296 eruptions were stacked in $\delta^{18}\text{O}$ of 13 cores ($\delta^{18}\text{O}_{\text{ice}}$), as well as $\delta^{18}\text{O}_{\text{reconst}}$ and SLP field reconstructions
297 to retrieve a composite anomaly signal 0-5 years after NH eruptions. T2m fields can be found in
298 supplementary Figure F6. As for the EQ eruptions, the post-volcanic reconstruction fields are assessed
299 by using the average $\delta^{18}\text{O}$ and surface pressure pattern associated with each weather regime
300 (supplementary Table T3-T4).

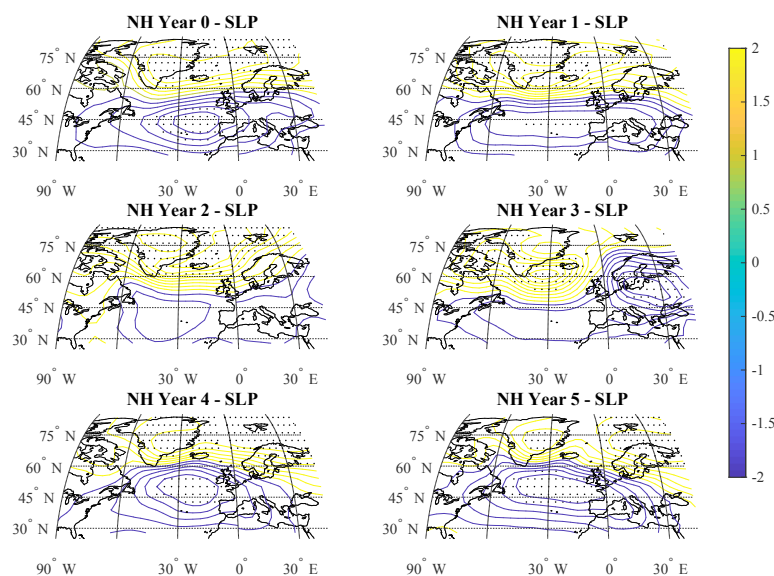
301



302
303 Figure 7: Composite $\delta^{18}\text{O}$ anomalies of 13 Greenland ice cores (1771-1970 CE) 0-5 years after 5 North
304 Hemisphere volcanic eruptions.
305
306



307
308 Figure 8: The short-term $\delta^{18}\text{O}$ response 0-5 years after 5 NH volcanic eruptions.
309



310
311 Figure 9: The surface pressure response 0-5 years after 5 NH volcanic eruptions.

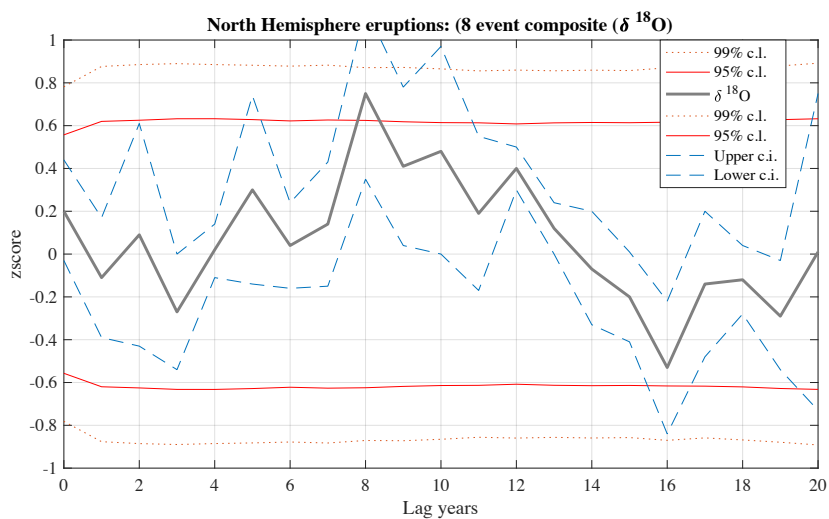
312
313 The pattern emerging in the $\delta^{18}\text{O}_{\text{ice}}$ (Figure 7) is in agreement with $\delta^{18}\text{O}_{\text{reconst}}$ (Figure 8) where negative
314 anomalies develop in years 1-3 followed by positive anomalies in years 4-5. $\delta^{18}\text{O}_{\text{ice}}$ is consistent with
315 $\delta^{18}\text{O}_{\text{reconst}}$ and SLP in years 1 and 2 where a clear NAO- emerges ($\delta^{18}\text{O}_{\text{ice}}$: $r=0.65$ and 0.66 respectively,
316 SLP: $r=0.96$ and 0.89 respectively). In year 3, AtR is present in both fields ($r=0.67$ and $r=0.71$). This is
317 consistent with the negative anomalies detected in the $\delta^{18}\text{O}_{\text{ice}}$ in years 1-3 and become significant in
318 years 2 (95% c.l.) and year 3 (90% c.l.). In years 4-5 clear positive anomalies emerges in $\delta^{18}\text{O}_{\text{ice}}$ that is
319 expected during an NAO+, also displayed in $\delta^{18}\text{O}$, while NAO- is present in SLP. The $\delta^{18}\text{O}_{\text{ice}}$ for years
320 4 and 5 show positive anomalies at almost all sites that become significant at the 95% c.l. at two sites
321 in year 5 (Figure 4) and 90% significant at Dye 3. These positive anomalies are also captured in $\delta^{18}\text{O}$
322 and T2m (Figures 5 and Figure F4) where the pattern correlates weakly to both ScB and NAO-.

323
324 **3.2.2 Atmospheric circulation response 2-5, 8-10 and 16 years after NH eruptions: 1241-1978 CE**
325 Figures 10-12 show results for the atmospheric circulation response where the significant years
326 detected in the 3-core average (Figure 4a) have been retrieved from the reconstruction fields.
327 Anomalies are calculated with respect to 10 years prior to each event. The volcanic eruptions were
328 selected according to Table 1 where volcanic eruptions were stacked to retrieve the volcanic signal in
329 $\delta^{18}\text{O}_{\text{ice}}$ of 3 cores, as well as $\delta^{18}\text{O}_{\text{reconst}}$ and SLP, to retrieve a composite anomaly signal 2-5, 8-10 and
330 16 years after NH eruptions. To avoid mixing with large EQ eruptions, only 7 NH volcanic eruptions
331 are stacked to retrieve the long-term response compared to 8 volcanic eruptions that are stacked to
332 retrieve the short-term response. See T2m post volcanic fields in supplementary Figure F5 and
333 supplementary Table T3-T4.

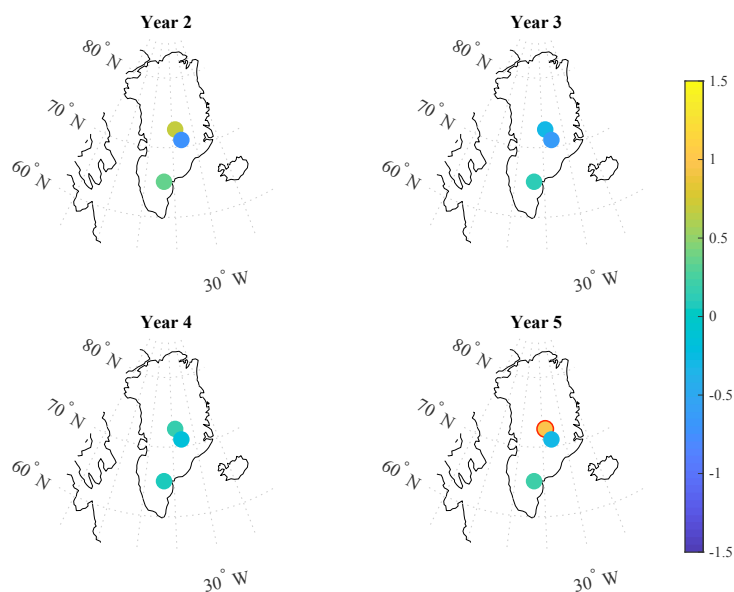
334



335
336 a)



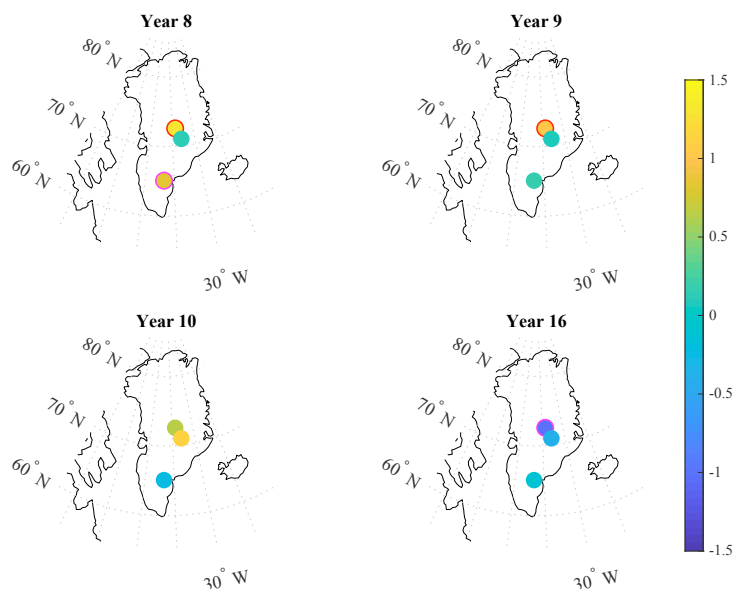
337
338
339 b)



340
341
342
343
344
345

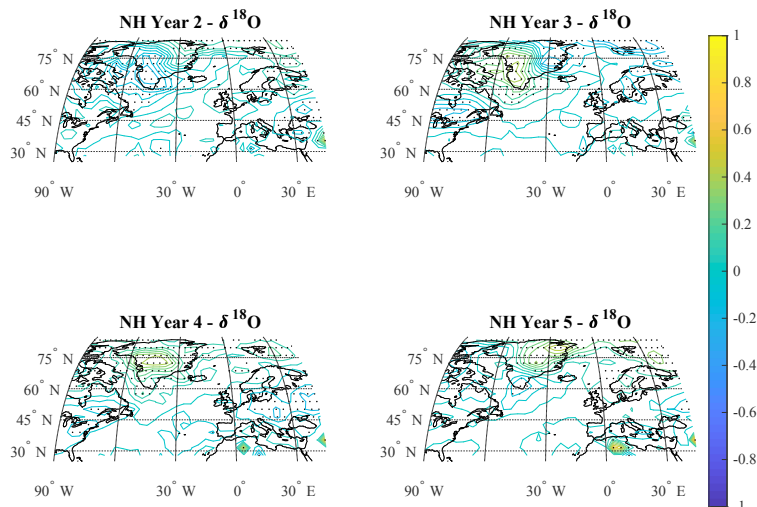


346
347 c)



348
349 Figure 10: a) The short-term and b) long-term $\delta^{18}\text{O}$ response after 8 and 7 NH volcanic eruptions
350 respectively, retrieved by stacking 3 Greenland ice cores spanning 1241-1978 CE. In c) the $\delta^{18}\text{O}$
351 retrieved by averaging Dye 3, GRIP and Crete is illustrated, where the red circle refers to a year of 95%
352 significance according to a Student's t-test and the cyan circles are 90% significant.

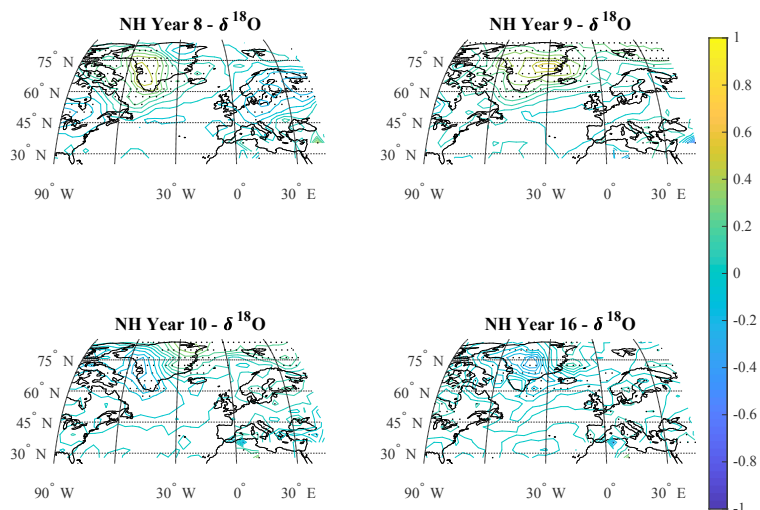
353
354 a)



355
356

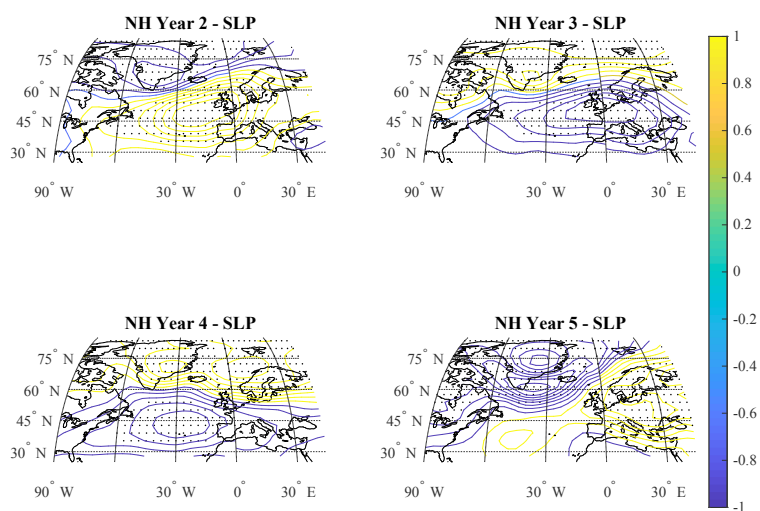


357
358 b)



359
360 Figure 11: The reconstructed $\delta^{18}\text{O}$ fields a) 2-5 years and b) 8-10 and 16 years after 8 and 7 NH
361 volcanic eruptions, respectively.

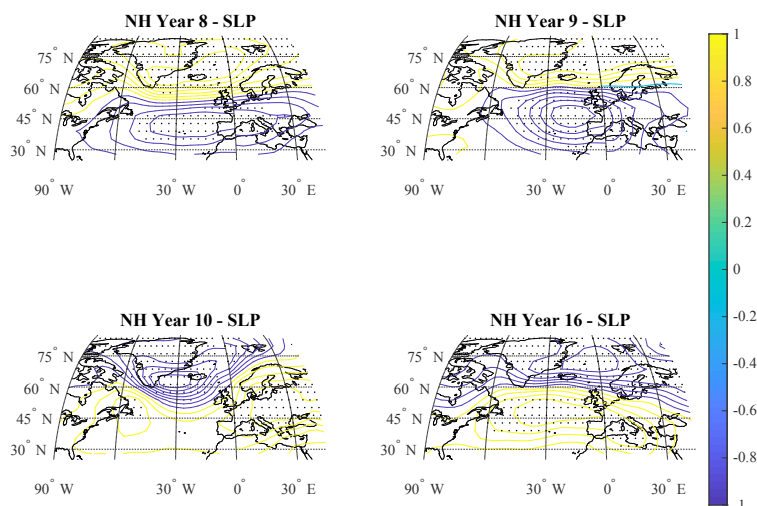
362
363 a)



364
365
366
367
368
369



370
371 b)



372
373 Figure 12: The reconstructed $\delta^{18}\text{O}$ fields a) 2-5 years and b) 8-10 and 16 years after 8 and 7 NH
374 volcanic eruptions, respectively.

375
376 The spatial $\delta^{18}\text{O}_{\text{ice}}$ pattern in Figure 10 shows a consistent relationship with the pattern emerging over
377 Greenland in $\delta^{18}\text{O}_{\text{reconst}}$ (Figure 11). In Figure 10a the atmospheric circulation response that emerges in
378 the $\delta^{18}\text{O}_{\text{ice}}$ anomalies is not as clear as compared to Figure 7, where year 5 is only significant at the
379 95% c.l. In $\delta^{18}\text{O}_{\text{reconst}}$ and SLP fields (Figures 11a and 12a respectively), using a composite of 8
380 eruptions, ScB emerges in year 2 ($r=0.57$) while NAO+ emerges in the SLP ($r=0.78$). NAO- emerges in
381 both the $\delta^{18}\text{O}$ and SLP ($r=0.86$ and $r=0.68$ respectively) in year 3 ($r=0.86$ and $r=0.56$ respectively) and
382 4 ($r=0.56$ and $r=0.86$ respectively). Similar to year 2, ScB emerges in the reconstructed $\delta^{18}\text{O}$ ($r=0.69$) in
383 year 5 while NAO+ is present in the SLP ($r=0.60$). The T2m fields provide a support for the $\delta^{18}\text{O}_{\text{reconst}}$,
384 suggesting that ScB and NAO- are dominating in the first 5 years after NH eruptions.

385 Years 8 and 9 (Figure 11b and 12b) show $\delta^{18}\text{O}_{\text{ice}}$ anomalies significant in the 95% c.l. being present at
386 GRIP as well as 90% significant at Dye 3 in year 8. These positive anomalies of year 8 are associated
387 with a clear NAO- being present in both $\delta^{18}\text{O}$ ($r=0.84$) and SLP ($r=0.95$), also present in the
388 reconstructions of year 9 ($r=0.49$ and $r=0.79$ respectively). As for year 2 and 5, year 10 has an ScB
389 present in $\delta^{18}\text{O}_{\text{reconst}}$ ($r=0.63$) while NAO+ is present in SLP ($r=0.76$). On average, the SLP fields detect
390 NAO+ or NAO- more frequent compared to ScB or AtR. This is not the case for the other fields
391 ($\delta^{18}\text{O}_{\text{reconst}}$ and T2m) and therefore the SLP is perhaps more sensitive towards NAO compared to the
392 other regimes. A clear NAO+ emerges in year 16 in the reconstructions ($\delta^{18}\text{O}$: $r=0.43$, SLP: $r=0.90$) as
393 well as significant negative anomalies being present in $\delta^{18}\text{O}_{\text{ice}}$, a further evidence for the presence of
394 NAO+.

395
396



397 4 Discussions & conclusions

398 The results show a consistent atmospheric circulation response in years 1-4 after EQ volcanic eruptions
399 in both the reconstructions of Sjolte et al. (2018) and $\delta^{18}\text{O}$ of Greenland ice cores, where both AtR and
400 NAO+ emerge in the first four years after an eruption. An increase in the frequency of AtR was also
401 detected in year 2 after EQ eruptions using six ECHAM5 ensemble members (including ECHAM5-
402 wiso) in Guðlaugsdóttir et al. (2018) where the authors concluded that the signal emerges as a result of
403 volcanic surface cooling. According to ECHAM5-wiso, a $\delta^{18}\text{O}$ gradient is present over the Greenland
404 during an AtR with negative anomalies present in the NE part of Greenland that becomes positive
405 towards Baffin Island in the SW. The opposite occurs during NAO+, where more positive anomalies
406 are present in the NE while more negative anomalies are present in the SW where the gradient (the
407 $\delta^{18}\text{O}$ difference between NE and SW) is stronger during NAO+. This difference is not clear when it
408 comes to the identification of AtR in $\delta^{18}\text{O}_{\text{ice}}$, where more data from sites further north would benefit the
409 identification agreeing with Guðlaugsdóttir et al. (2019). The significance of the negative $\delta^{18}\text{O}_{\text{ice}}$
410 anomalies of years 3-5 using a 5 EQ eruption composite, along with results from the reconstructions
411 (Figure 1-3), clearly indicate an NAO+ that is more prolonged than the expected NAO+ signal in the
412 first 2 years (Robock and Mao, 1992; Graf et al., 1994; Kodera, 1994; Fisher et al., 2007; Ortega et al.,
413 2015). Although this NAO+ signal is not as clear in the $\delta^{18}\text{O}_{\text{ice}}$ using 8 a composite of EQ eruption,
414 $\delta^{18}\text{O}_{\text{ice}}$ becomes significant in year 3 where all years show negative anomalies. However, as mentioned,
415 this does not rule out the presence of AtR in $\delta^{18}\text{O}_{\text{ice}}$. This prolonged NAO+ signal was previously
416 reported by Sjolte et al. (2018) where they identified an increase in the NAO index in the first five
417 years after EQ eruptions. Therefore similar results should be assumed. Furthermore, in Guðlaugsdóttir
418 et al. (2018) an increase in the frequency of NAO+ was identified 3-5 years after EQ eruptions. It has
419 been suggested that the volcanic surface cooling is overestimated in ECHAM5 (Driscoll et al., 2012)
420 where the model has failed to produce an NAO+ in the first two years after EQ eruptions, as would
421 otherwise be expected. However, an NAO+ is identified in the reconstructions in years 1-5 and
422 therefore they do not seem to depend on this volcanic sensitivity that seem to be present in ECHAM5.
423 To answer if this AtR response in years 2 and 4 is indeed a natural response to large EQ eruptions,
424 more data and analysis is required. The identification of this prolonged NAO+ pattern in $\delta^{18}\text{O}_{\text{ice}}$ is
425 important in order to establish a mechanism behind such a delayed response. Both the $\delta^{18}\text{O}$ and T2m in
426 Figures 2a, 5a and F2 and F3 provide us with evidence of a temperature decrease in the Nordic Seas
427 that would again be in support of the known sea ice increase after EQ eruptions in that region. This sea
428 ice increase could lead to NAO+ via an increase in planetary wave formation and transport, where it is
429 known that the opposite occurs during a sea ice decrease leading to NAO- (Kim et al., 2014;
430 Magnúsdóttir et al., 2004). In our case it seems that although an increased latitudinal temperature
431 difference in the stratosphere initially leads to NAO+ in year 1, the NAO+ remains to be persistent as a
432 result of an increase in planetary wave formation. However, the AtR also participates in this climate
433 response as a result of surface cooling. The strength of this prolonged NAO+ response seems to depend
434 on the number of volcanic eruptions being stacked, where the 5 EQ eruptions composite results in a
435 stronger and more persistent NAO+ signal (years 1-2 and 4-5) compared to the 8 EQ eruption
436 composite (years 1 and 3). AtR emerges using both 5 (year 3) and 8 composite EQ eruptions (2 and 4).



437 The volcanic signal 8-11 years after EQ eruption is clear in $\delta^{18}\text{O}_{\text{ice}}$ where negative anomalies are in
438 support of the persistent NAO+ present in the reconstruction fields. The significance of year 10 when
439 the cores are averaged also provides a support for the detected NAO+ (Figure 6c). Zanchettin et al.
440 (2012) identified a similar volcanic response as a winter warming, where NAO+ emerged in years 10-
441 12, while Guðlaugsdóttir et al. (2018) identified the emergence of NAO+ two years later. This timing
442 also agrees with the known decadal increase in Atlantic Meridional Overturning Circulation (AMOC)
443 identified in Swingedouw et al. (2015). The response detected in years 17-20 is not as robust compared
444 to previous years analyzed. However, a robust NAO- response emerges in year 17 as a significant
445 negative $\delta^{18}\text{O}_{\text{ice}}$ anomaly at GRIP and in the pattern detected in reanalysis fields. This is followed by a
446 significant negative $\delta^{18}\text{O}_{\text{ice}}$ anomaly at Dye 3 that is evidence for the presence of NAO+ as is detected
447 in SLP in year 18 and 19. According to Swingedouw et al. (2015), an increase in North Atlantic SST
448 (25-55°N) reaches a maximum around year 20, occurring at the time of a slight weakening detected in
449 the AMOC. We do not see evidence for this SST increase in our $\delta^{18}\text{O}$ and T2m fields although the
450 presence of NAO+ in $\delta^{18}\text{O}_{\text{ice}}$ and SLP does indicate a warming pattern over the Northern Hemisphere
451 landmass. However, the causality between our results and a weakening of the ocean gyre circulation
452 (AMOC) can only be speculative at this stage.

453
454 The atmospheric circulation response 0-5 years after NH eruptions according to our results emerges as
455 a robust NAO- response in years 1 and 2 by using 5 NH eruption composite while NAO- emerges in
456 year 3 and 4 using 8 eruption composite. In both year 2 and 5, NAO+ is detected in the SLP but ScB in
457 the $\delta^{18}\text{O}$. While the reconstructed SLP fields result in an NAO+ or NAO- like pattern for almost all
458 years analyzed for both NH and EQ eruptions (an exception being year 2, 4 and 20 after EQ eruptions),
459 the same is not to be said regarding the reconstructed $\delta^{18}\text{O}$ and T2m fields. When the clustering
460 method, also used on the SLP of ECHAM5-wiso (K-means clustering, $k=4$), is used on the
461 reconstructed SLP only NAO emerges (not shown). It therefore seems that years when ScB emerges in
462 the $\delta^{18}\text{O}$ the SLP detects it as NAO+ (year 2 and 5 after NH eruptions as well as year 18 after EQ
463 eruptions), since the SLP has a tendency towards NAO although it is able to detect AtR. When the
464 $\delta^{18}\text{O}_{\text{ice}}$ is considered, both for 5 and 8 NH eruption composite, our results are more in favor of ScB,
465 especially for year 5. This is in agreement with Guðlaugsdóttir et al. (2018) that suggests that weather
466 regimes that are associated with a weaker stratospheric polar vortex, like AtR, ScB and NAO-, are
467 more common in the first years after NH volcanic eruptions compared to NAO+ that is evident of a
468 stronger polar vortex. It was first proposed by Graf et al. (1994) that NH eruptions could weaken the
469 stratospheric polar vortex due to the decrease in meridional (latitudinal) temperature gradient. The
470 identification of weather regimes associated with such a polar vortex weakening provides an
471 opportunity to forecast potential extreme events in the aftermath of NH eruptions, where it can be
472 assumed based on our results that such eruptions do not need to be as large as EQ eruptions to have an
473 impact. The long-term atmospheric circulation response after NH eruptions according to our results is a
474 robust NAO- in years 8 and 9. Again, the SLP detects NAO+ in year 10 while $\delta^{18}\text{O}$ detects ScB. When
475 the $\delta^{18}\text{O}_{\text{ice}}$ is considered, the pattern emerging in year 10 is more in favor of ScB but this pattern is not
476 significant. Year 16 results in a robust NAO+ pattern in both the $\delta^{18}\text{O}_{\text{ice}}$ and the reconstruction fields.



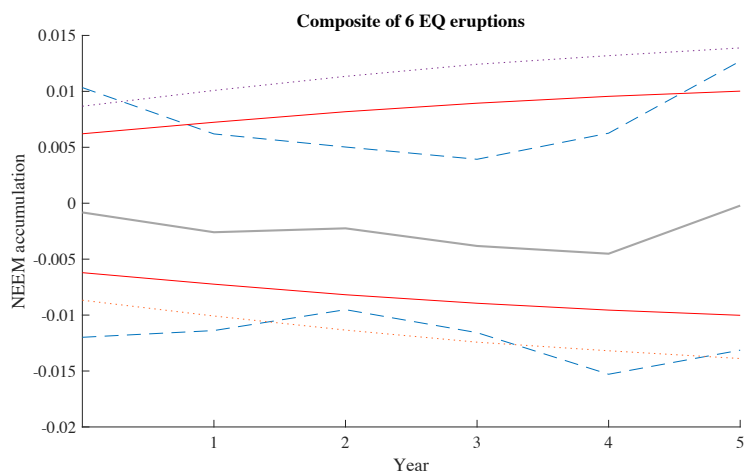
477 The key to answer questions regarding the long-term (decadal/multi-decadal) response lie within the
478 ocean and sea ice response to volcanic eruptions, and since these components are outside of the scope
479 of this study we can only speculate about the possible mechanism. In a study by Pausata et al. (2015) a
480 sudden decrease in the Ocean Heat Content was reported in the first 5 years due to the volcanic surface
481 cooling after high latitude eruptions. The OHC increased slowly until year 10-15 where it reached a
482 steady state (below average) throughout the study period. This offers one explanation to the emerging
483 NAO+ in year 16 after NH eruptions, where the OHC increase result in an NAO+ -like SST pattern. It
484 can be observed in the reconstructed $\delta^{18}\text{O}$ fields that the area over Greenland is significant in all years
485 analyzed, both for EQ and NH eruptions (Figures 2, 5, 8 and 11), indicating a bias in the
486 reconstructions towards Greenland since it is less significant towards the northern mid latitudes.
487 However, it is unlikely that this bias would favor any particular weather regime although the centers of
488 action in the weather regimes may show tendencies towards the Greenland ice sheet that would
489 otherwise vary.

490 The pattern that appears to be emerging here is a difference in the atmospheric circulation response
491 after EQ eruptions compared to the response after NH eruptions, where NAO+ and AtR seems to be
492 more associated with EQ eruptions while NAO- and ScB seems to follow NH eruptions. To assess this
493 anti-phase in the response of EQ and NH eruptions, we move further north over the Greenland ice sheet
494 to study the accumulation in the shallow ice cores of NEEM and test if a difference in accumulation
495 can be detected. Although ~70% of the accumulation at NEEM falls during summer, NEEM offers the
496 possibility to examine this further. When the basic definition of the different phases of NAO is
497 considered in terms of precipitation amount, NAO+ is on average associated with less precipitation
498 over Greenland while NAO- is associated with more precipitation (Hurrell, 1995). Our results, done by
499 stacking six EQ and NH volcanic eruptions (see Table 1) in similar manner as above, are presented in
500 Figure 13 where this relationship is only weakly indicated. The accumulation decreases slightly in
501 years 1-4 where the NAO index (gray and blue dashed lines) remains below the 95% threshold,
502 indicating a slight accumulation decrease. A slight increase is observed in the trend of the lower c.i.
503 (blue dashed line) after NH eruptions in years 1-4 where the upper 95% c.i. remains above the 95%
504 threshold. However these changes are weak in our results and the question regarding precipitation
505 changes after both EQ and NH volcanic eruption and if it can be associated with the two different
506 phases of NAO (as well as AtR and ScB) demands more data before it can be answered.

507
508
509
510
511
512
513
514
515
516

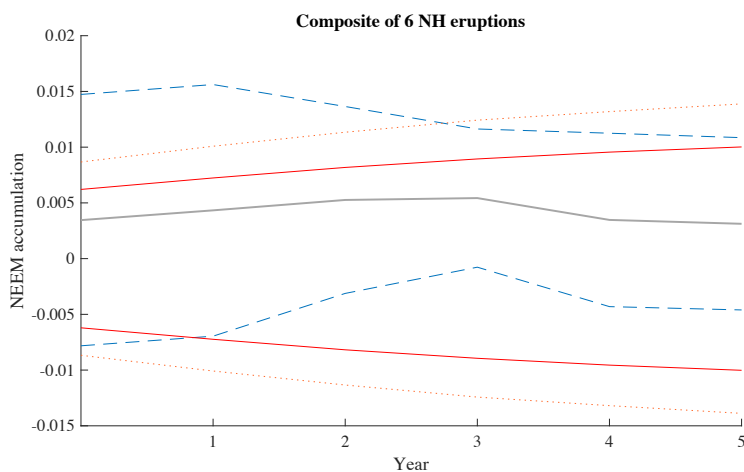


517 a)



518

519 b)



520

521

522 Figure 13: The composite volcanic response in the accumulation at NEEM 0-5 years after an eruption
523 using a) 6 EQ and b) 6 NH volcanic eruptions, where anomalies are calculated with respect to 10 years
524 prior each eruption. Grey lines indicate the average NAO index, the blue dashed lines are upper and
525 lower 95% c.i. The red line indicate 95% c.i. and the orange 99% c.i. that is calculated by methods of
526 Monte Carlo.

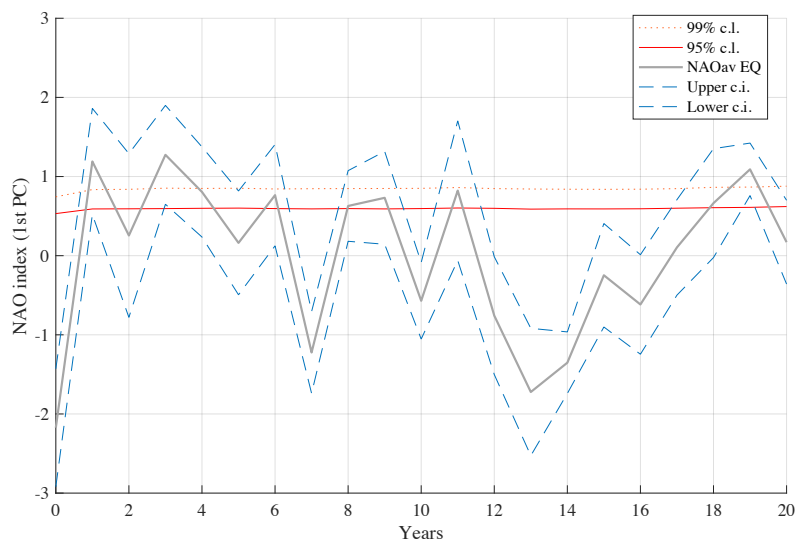
527

528 This can also be observed in the NAO index, derived from the 1st PC of the reconstructed SLP. In
529 Figure 14a and 14b, 8 EQ and 8/7 NH volcanic eruptions (see Table 1) are stacked to retrieve a
530 common response in the NAO. There the decadal-to-multidecadal response is quite strong after both
531 EQ and NH eruptions. Furthermore, what is of interest is that years with low $\delta^{18}\text{O}$ (Figure 4a and 10a)



532 coincide with years of high NAO index (NAO+) and vice versa (Figure 14). This is particularly clear
533 for year 8 and 16 after NH eruptions while the first five years in the average $\delta^{18}\text{O}_{\text{ice}}$ (Figure 10a) do not
534 show clear evidence for NAO- compared to Figure 14b.
535 NH eruptions seem to leave a slightly more persistent NAO response for reasons we can only speculate
536 at this stage. However, this does not rule out other regimes being present in these first 5 years after an
537 eruption, e.g. AtR after EQ eruptions or ScB after NH eruptions although the the NAO seems to be the
538 dominating the atmospheric circulation response. According to these results, EQ eruptions cause a clear
539 shift in the NAO index baseline, where a sudden increase occurs in year 1 after EQ eruptions. Although
540 the sudden significant decrease in year 7 and 13 is evidence of an atmospheric response it could also be
541 the system rebalancing. NAO index seems to oscillate more after NH eruptions. This is evident of a
542 weaker NAO response after NH eruptions as a result of a higher internal variability that emerges when
543 the NH eruptions are stacked. However, since similar trends are observed in the ice cores this suggest a
544 climate response forced by NH eruptions.

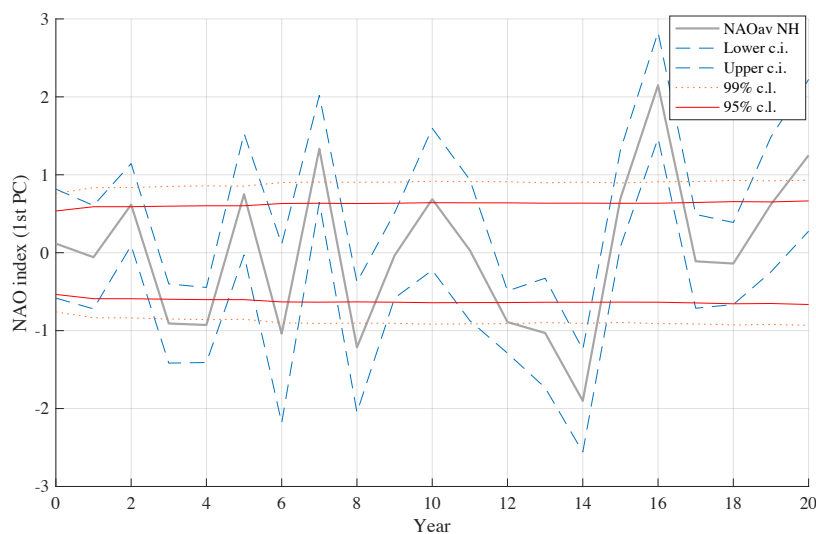
545
546 a)



547
548
549
550
551
552
553
554
555
556
557



558 b)



559

560 Figure 14: a) The normalized NAO index after the stacking of 8 EQ eruptions and b) the same but after
561 the stacking of 8 (first 5 years) and 7 (years 6-20) NH eruptions. The red and orange c.l. are calculated
562 by methods of Monte Carlo.

563

564 Although this study aims to complement the understanding of the atmospheric circulation response
565 after volcanic eruptions, as well as differentiating between the response after EQ and NH eruptions,
566 two important factors of the climate system are not within the scope of this study. These factors are the
567 ocean and sea ice, where changes in one can influence the other on a decadal to centennial time scales.
568 The mechanism behind the NAO- response we detect after NH eruptions may well lie in the sea ice
569 response to volcanic eruptions that we do not explore, especially when the results of Figure 13 are
570 taken into consideration. It is known that sea ice cover extent influences the planetary wave formation
571 by weakening the stratospheric zonal winds and therefore gives rise to NAO- (Kim et al., 2014;
572 Magnúsdóttir et al., 2004). This has especially been observed in relation with anthropogenic forcing,
573 where the decline in sea ice extent as a result of average global temperature increase has resulted in
574 more frequent presence of NAO- as well as ScB (Dobricic et al., 2016; Budikova, 2009 and references
575 therein). Therefore the understanding on the behavior of the climate system after volcanic eruptions can
576 serve to understand future changes in climate variability due to anthropogenic forcing and raises
577 questions regarding the potential positive climate feedback of NH eruptions. Furthermore, the
578 sensitivity of the climate system (the atmosphere, ocean and sea ice) towards NH eruptions, like e.g.
579 size and type of the eruption as well as the season in which the eruption occurs, remains to be assessed
580 in details and will be left for future studies.

581

582

583



584 **References**

- 585 Budikova, D.: Role of Arctic sea ice in global atmospheric circulation: A review. *Global and Planetary*
586 *Change*, 68, 149-163, 2009.
- 587 Cassou, C., Terray, L., Hurrell, J. W., and Deser, C.: North Atlantic winter climate regimes: Spatial
588 asymmetry, stationarity with time, and oceanic forcing. *Journal of Climate*, 17, 1055-1068, 2004.
- 589 Carey, R. J., Houghton, B. F., and Thordarson, T.: Abrupt shifts between wet and dry phases of the
590 1875 eruption of Askja Volcano: microscopic evidence for macroscopic dynamics. *Journal of*
591 *Volcanology and Geothermal Research*, 184, 256-270, 2009.
- 592 Dobricic, S., Vignati, E., and Russo, S.: Large-scale atmospheric warming in winter and the Arctic sea
593 ice retreat. *Journal of Climate*, 29, 2869-2888, 2016.
- 594 Driscoll, S., Bozzo, A., Gray, L. J., Robock, A., and Stenchikov, G.: Coupled Model Intercomparison
595 Project 5 (CMIP5) simulations of climate following volcanic eruptions. *Journal of Geophysical*
596 *Research: Atmospheres*, 117, 2012.
- 597 Fischer, E. M., Luterbacher, J., Zorita, E., Tett, S. F. B., Casty, C., and Wanner, H.: European climate
598 response to tropical volcanic eruptions over the last half millennium. *Geophysical Research Letters*,
599 34, 2007.
- 600 Graf, H. F., Perlwitz, J., and Kirchner, I.: Northern hemisphere tropospheric midlatitude circulation
601 after violent volcanic eruptions. *Contr. Atmos. Physics*, 67, 3–13, 1994.
- 602 Guðlaugsdóttir, H., Steen-Larsen, H. C., Sjolte, J., Masson-Delmotte, V., Werner, M., and
603 Sveinbjörnsdóttir, Á. E.: The influence of volcanic eruptions on weather regimes over the North
604 Atlantic simulated by ECHAM5/MPI-OM ensemble runs from 800 to 2000 CE. *Atmospheric*
605 *Research*, 2018.
- 606 Guðlaugsdóttir, H., Sjolte, J., Sveinbjörnsdóttir, Á. E., Werner, M., & Steen-Larsen, H. C.: North Atlantic
607 weather regimes in $\delta^{18}\text{O}$ of winter precipitation: isotopic fingerprint of the response in the atmospheric
608 circulation after volcanic eruptions. *Tellus B: Chemical and Physical Meteorology*, 71, 1-19, 2019.
- 609 Hurrell, J. W.: Decadal trends in the north atlantic oscillation: regional temperatures and precipitation.
610 *Science*, 269, 676–679, 1995.
- 611 Janebo, M. H., Thordarson, T., Houghton, B. F., Bonadonna, C., Larsen, G., and Carey, R. J.: Dispersal
612 of key subplinian–Plinian tephra from Hekla volcano, Iceland: implications for eruption source
613 parameters. *Bulletin of Volcanology*, 78, 66, 2016.
- 614 Jungclauss, J. H., Lorenz, S. J., Timmreck, C., Reick, C. H., Brovkin, V., Six, K., Segschneider, J.,
615 Giorgetta, M.A., Crowley, T.J., Pongratz, J., and Krivova, N. A.: Climate and carbon-cycle
616 variability over the last millennium. *Climate of the Past*, 6, 723-737, 2010.
- 617 Johnsen, S.J., Dahl-Jensen, D., Gundestrup, N., Steffensen, J.P., Clausen, H.B., Miller, H., Masson-
618 Delmotte, V., Sveinbjörnsdóttir, A.E., and White, J.: Oxygen isotope and palaeotemperature records
619 from six Greenland ice-core stations: Camp Century, Dye-3, GRIP, GISP2, Renland and NorthGRIP.
620 *Journal of Quaternary Science: Published for the Quaternary Research Association*, 16, 299-307,
621 2001.



- 622 Jouzel, J., Alley, R.B., Cuffey, K.M., Dansgaard, W., Grootes, P., Hoffmann, G., Johnsen, S.J., Koster,
623 R.D., Peel, D., Shuman, C.A., and Stievenard, M.: Validity of the temperature reconstruction from
624 water isotopes in ice cores. *Journal of Geophysical Research: Oceans*, 102, 26471-26487, 1997.
- 625 Kim, B. M., Son, S. W., Min, S. K., Jeong, J. H., Kim, S. J., Zhang, X., Shim, T., and Yoon, J. H.:
626 Weakening of the stratospheric polar vortex by arctic sea-ice loss. *Nature communications*, 5, 4646,
627 2014.
- 628 Kodera, K.: Influence of volcanic eruptions on the troposphere through stratospheric dynamical
629 processes in the northern hemisphere winter. *Journal of Geophysical Research: Atmospheres*, 99,
630 1273–1282, 1994.
- 631 Magnusdottir, G., Deser, C., and Saravanan, R.: The effects of north atlantic SST and sea ice anomalies
632 on the winter circulation in CCM3. part i: Main features and storm track characteristics of the
633 response. *Journal of Climate*, 17, 857–876, 2004.
- 634 Muscheler, R., Adolphi, F., Herbst, K., and Nilsson, A.: The revised sunspot record in comparison to
635 cosmogenic radionuclide-based solar activity reconstructions. *Solar Physics*, 291, 3025-3043, 2016.
- 636 Ortega, P., Swingedouw, D., Masson-Delmotte, V., Risi, C., Vinther, B., Yiou, P., Vautard, R., and
637 Yoshimura, K.: Characterizing atmospheric circulation signals in Greenland ice cores: insights from a
638 weather regime approach. *Climate dynamics*, 43, 2585-2605, 2014.
- 639 Ortega, P., Lehner, F., Swingedouw, D., Masson-Delmotte, V., Raible, C. C., Casado, M., and Yiou,
640 P.: A model-tested North Atlantic Oscillation reconstruction for the past millennium. *Nature*, 523, 71,
641 2015.
- 642 Otterå, O. H., Bentsen, M., Drange, H., and Suo, L.: External forcing as a metronome for Atlantic
643 multidecadal variability. *Nature Geoscience*, 3, 688, 2010.
- 644 Pausata, F. S., Chafik, L., Caballero, R., and Battisti, D. S. (2015). Impacts of high-latitude volcanic
645 eruptions on ENSO and AMOC. *Proceedings of the National Academy of Sciences*, 112, 13784-
646 13788, 2015.
- 647 Petit, J.R., Jouzel, J., Raynaud, D., Barkov, N.I., Barnola, J.M., Basile, I., Bender, M., Chappellaz, J.,
648 Davis, M., Delaygue, G. and Delmotte, M.: Climate and atmospheric history of the past 420,000
649 years from the Vostok ice core, Antarctica. *Nature*, 399, 429, 1999.
- 650 Robock, A., and Mao, J.: Winter warming from large volcanic eruptions. *Geophysical Research*
651 *Letters*, 19, 2405-2408, 1992.
- 652 Sharma, K., Self, S., Blake, S., Thordarson, T., and Larsen, G.: The AD 1362 Öræfajökull eruption, SE
653 Iceland: Physical volcanology and volatile release. *Journal of Volcanology and Geothermal Research*,
654 178, 719-739, 2008.
- 655 Sigl, M., Winstrup, M., McConnell, J. R., Welten, K. C., Plunkett, G., Ludlow, F., Büntgen, U., Caffee,
656 M., Chellman, N., Dahl-Jensen, D., and Fischer, H.: Timing and climate forcing of volcanic eruptions
657 for the past 2,500 years. *Nature*, 523, 543, 2015.
- 658 Sjolte, J., Sturm, C., Adolphi, F., Vinther, B. M., Werner, M., Lohmann, G. and Muscheler, R.: Solar
659 and volcanic forcing of North Atlantic climate inferred from a process-based reconstruction, *Clim.*
660 *Past*, 14, 1179-1194, 2018.



661 Swingedouw, D., Ortega, P., Mignot, J., Guilyardi, E., Masson-Delmotte, V., Butler, P. G., Khodri, M.,
662 and Séférian, R.: Bidecadal North Atlantic ocean circulation variability controlled by timing of
663 volcanic eruptions. *Nature communications*, 6, 6545, 2015.

664 Thordarson, T. and Self, S.: Atmospheric and environmental effects of the 1783–1784 Laki eruption: A
665 review and reassessment. *Journal of Geophysical Research: Atmospheres*, 108, 2003.

666 Thordarson, T., and Larsen, G.: Volcanism in Iceland in historical time: Volcano types, eruption styles
667 and eruptive history. *Journal of Geodynamics*, 43, 118-152, 2007.

668 Vinther, B. M., Jones, P. D., Briffa, K. R., Clausen, H. B., Andersen, K. K., Dahl-Jensen, D., and
669 Johnsen, S. J.: Climatic signals in multiple highly resolved stable isotope records from Greenland.
670 *Quaternary Science Reviews*, 29, 522-538, 2010.

671 Wallace, J. M. and Gutzler, D. S.: Teleconnections in the geopotential height field during the Northern
672 Hemisphere winter. *Monthly Weather Review*, 109, 784-812, 1981.

673 Werner, M., Haese, B., Xu, X., Zhang, X., Butzin, M., and Lohmann, G.: Glacial–interglacial changes
674 in H218O, HDO and deuterium excess—results from the fully coupled ECHAM5/MPI-OM Earth
675 system model. *Geoscientific Model Development*, 9, 647-670, 2016.

676 Zanchettin, D., Timmreck, C., Graf, H. F., Rubino, A., Lorenz, S., Lohmann, K., Krüger, K., and
677 Jungclaus, J. H.: Bi-decadal variability excited in the coupled ocean–atmosphere system by strong
678 tropical volcanic eruptions. *Climate Dynamics*, 39, 419-444, 2012.

679
680
681
682
683
684
685
686
687
688
689
690
691